On the physics of multidrug efflux through a biomolecular complex.

AUTHOR(S):

Mishima, Hirokazu; Oshima, Hiraku; Yasuda, Satoshi; Amano, Ken-Ichi; Kinoshita, Masahiro

CITATION:

Mishima, Hirokazu ...[et al]. On the physics of multidrug efflux through a biomolecular complex.. The Journal of chemical physics 2013, 139(20): 205102.

ISSUE DATE:

2013-11-27

URL:

http://hdl.handle.net/2433/179789

On the physics of multidrug efflux through a biomolecular complex

Hirokazu Mishima, Hiraku Oshima, Satoshi Yasuda, Ken-ichi Amano, and Masahiro Kinoshita

Citation: The Journal of Chemical Physics **139**, 205102 (2013); doi: 10.1063/1.4832896
View online: http://dx.doi.org/10.1063/1.4832896
View Table of Contents: http://scitation.aip.org/content/aip/journal/jcp/139/20?ver=pdfcov
Published by the AIP Publishing

THE JOURNAL OF CHEMICAL PHYSICS **139**, 205102 (2013)

On the physics of multidrug efflux through a biomolecular complex

Hirokazu Mishima,[1] Hiraku Oshima,[2] Satoshi Yasuda,[2] Ken-ichi Amano,[3] and Masahiro Kinoshita[2,a)]

[1]*Graduate School of Energy Science, Kyoto University, Uji, Kyoto 611-0011, Japan*
[2]*Institute of Advanced Energy, Kyoto University, Uji, Kyoto 611-0011, Japan*
[3]*Faculty of Pharmaceutical Sciences, Tohoku Pharmaceutical University, Komatsushima, Aoba-ku, Sendai 981-8558, Japan*

(Received 9 August 2013; accepted 7 November 2013; published online 27 November 2013)

Insertion and release of a solute into and from a vessel comprising biopolymers is a fundamental function in a biological system. A typical example is found in a multidrug efflux transporter. "Multidrug efflux" signifies that solutes such as drug molecules with diverse properties can be handled. In our view, the mechanism of the multidrug efflux is not chemically specific but rather has to be based on a physical factor. In earlier works, we showed that the spatial distribution of the solute-vessel potential of mean force (PMF) induced by the solvent plays imperative roles in the insertion/release process. The PMF can be decomposed into the energetic and entropic components. The entropic component, which originates from the translational displacement of solvent molecules, is rather insensitive to the solute-solvent and vessel inner surface-solvent affinities. This feature is not shared with the energetic component. When the vessel inner surface is neither solvophobic nor solvophilic, the solvents within the vessel cavity and in the bulk offer almost the same environment to any solute with solvophobicity or solvophilicity, and the energetic component becomes much smaller than the entropic component (i.e., the latter predominates over the former). Our idea is that the multidrug efflux can be realized if the insertion/release process is accomplished by the entropic component exhibiting the insensitivity to the solute properties. However, we have recently argued that the entropic release of the solute is not feasible as long as the vessel geometry is fixed. Here we consider a model of TolC, a cylindrical vessel possessing an entrance at one end and an exit at the other end for the solute. The spatial distribution of the PMF is calculated by employing the three-dimensional integral equation theory with rigid-body models in which the constituents interact only through hard-body potentials. Since the behavior of these models is purely entropic in origin, our analysis is focused on the entropic component. We show that the entropically inserted solute can be released by a continuous variation of the vessel geometry which forms a time-dependent entropic force continuing to accelerate the solute motion to the exit. Solutes with a wide range of sizes are entropically released using the same vessel-geometry variation. The results obtained are fairly general and also applicable to the efflux pump protein AcrB and ATP-binding cassette transporter. © *2013 AIP Publishing LLC*. [http://dx.doi.org/10.1063/1.4832896]

I. INTRODUCTION

Drug extrusion via efflux through a tripartite complex constructing the Resistance-Nodulation-Cell Division (RND) system is a widely used mechanism in Gram-negative bacteria. The complex comprises AcrA, AcrB, and TolC as illustrated in Fig. 1.[1–8] AcrB, which is referred to as an efflux pump protein, comprises three protomers. It has been suggested that each protomer undergoes a sequential structural change among three states in which a drug insertion, binding, and release take place, respectively.[5,6,8] The outer membrane protein, TolC, is a cylindrical vessel possessing an entrance at one end and an exit at the other end for the solute. The periplasmic linker protein, AcrA, mediates the contact between AcrB and TolC.[5,6,8] AcrB interacting with TolC in this way sends the solute to the central position within the vessel cavity of TolC at the entrance, and then the solute is moved to the exit. Thus, the transporter enables a passage of the drug from the periplasm to the external medium. A feature of the transporter is that it is capable of handling drugs with diverse properties (i.e., solvophobic and solvophilic solutes with a wide range of sizes).[6–8] This feature, which is known as "multidrug efflux," is in marked contrast with the high selectivity in the receptor-ligand binding. In our earlier works, it was shown that the high selectivity is ascribed to geometric characteristics of the receptor pocket and ligand, which are made substantial by the entropic effect originating from the translational displacement of solvent molecules.[9–11] Here, we show that the solvent-entropy effect plays crucially important roles in the multidrug efflux as well.

A prevailing view is the following: The multidrug efflux stems from multifunctional ligand-binding sites[4,5,12] of AcrB which recognize various types of functional groups; once the

a)Author to whom correspondence should be addressed. Electronic mail: kinoshit@iae.kyoto-u.ac.jp.

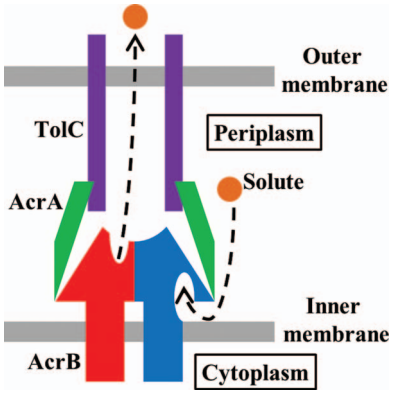

FIG. 1. Cartoon illustrating an efflux transporter, AcrA/AcrB/TolC.

solute enters TolC, it goes to the external medium merely by "diffusion"[12] in the presence of no particular potential field; and only AcrB is responsible for the multidrug efflux (in general, AcrB has caught more attention than TolC for analyses on the solute motion[12,13]). However, there is an important point to be noticed: Once AcrB sends the solute to the central position within the vessel cavity of TolC (the length of TolC reaches ∼14 nm that is far larger than the solute size) at the entrance, the solute must be ejected to the external medium through the exit before AcrB sends the next solute. The ejection of every solute needs to be finished with sufficient rapidness, but it is uncertain whether such ejection is achievable by the mere diffusion mentioned above or not. The achievement may be assured if the solute motion is directed only toward the exit (i.e., the solute motion is unidirectional). Also, we emphasize that the multidrug efflux of AcrA/AcrB/TolC can be realized only when TolC as well as AcrB exhibits this feature. TolC possesses an uncomplicated structure of a cylindrical shape with an open space inside it and works as a tunnel for drugs. The existence of the multifunctional ligand-binding sites can hardly be applied to TolC, implying that the multidrug efflux is implemented through a different mechanism. Further, it is not definite that such sites actually exist in AcrB. Even if they exist, a solute once bound to one of the sites is not likely to be released from it since the solute properties remain unchanged. The binding must be strong enough for the solute to remain captured, whereas it must be sufficiently weak for the solute dissociation in the next step. It is not straightforward to meet both of these requirements. In the present study, we revisit the mechanism of the multidrug efflux by considering TolC, from the standpoint that the mechanism cannot be chemically specific but rather has to be based on a physical factor. It is demonstrated that the multidrug efflux can be realized without assuming the existence of the multifunctional ligand-binding sites.

A principal concern is insertion of a solute into a vessel comprising biopolymers followed by release of the same solute from it. It is quite interesting that the two apparently *opposite* events, insertion and release, successively occur in a system. In earlier works,[14–17] we showed that the spatial distribution of the solute-vessel potential of mean force (PMF denoted by Φ) formed by the solvent plays imperative roles for the insertion/release process. The PMF represents "the free energy of the solvent for a fixed configuration of the solute-vessel pair" minus "that for the configuration where the solute is infinitely far from the vessel." The spatial distribution of the PMF becomes largely positive and largely negative with the periodicity of the molecular diameter of the solvent, $d_S = 0.28$ nm. The motion of a solute immersed in a solvent confined on the scale of a nanometer is influenced by the distribution.

It is physically insightful to decompose the PMF scaled by k_BT (k_B is Boltzmann's constant and T is the absolute temperature), $\Phi/(k_BT)$, into its energetic and entropic components denoted by $\Phi_E/(k_BT)$ and $-\Phi_S/k_B$, respectively: $\Phi/(k_BT) = \Phi_E/(k_BT) - \Phi_S/k_B$. In what follows, the conclusions drawn from our earlier works[15,16] are recapitulated. $\Phi_E/(k_BT)$ is strongly dependent on the solute-solvent and vessel inner surface-solvent affinities. When the inner surface of the vessel is solvophilic, the average solvent number density within the vessel cavity is higher than that in the bulk solvent. As a result, the solvent environment becomes more favorable within the cavity than in the bulk for a solvophilic solute, while the opposite is true for a solvophobic solute: The solvophilic solute is preferentially solvated within a small space almost in the center of the cavity but the solvophobic solute is more stabilized in the bulk. A solvophobic inner surface gives rise to a lower solvent number density on an average within the cavity, leading to preferential solvation of a solvophilic solute in the bulk and more stabilization of a solvophobic solute within the cavity. $-\Phi_S/k_B$, which originates from the translational displacement of solvent molecules, is rather insensitive to the solute-solvent and vessel inner surface-solvent affinities, namely, to whether the solute or the vessel inner surface is solvophobic or solvophilic (on condition that they are neither too solvophobic nor too solvophilic). It is closely related to the excluded volume (EV) generated by the solute. (The solute generates a space which the centers of solvent molecules cannot enter, and the volume of this space is the EV.) $-\Phi_S/k_B$ always drives the solute to be inserted into the vessel cavity and constrained within a small space almost in the center. The power of insertion and constraint becomes stronger as the EV increases. The release can be performed only by $\Phi_E/(k_BT)$.

In the protein flux through a chaperonin system,[15,16,18–20] where an unfolded protein is inserted into the chaperonin from the bulk solvent and the folded protein is released back to the bulk, the vessel properties (i.e., geometry and vessel inner surface-solvent affinity) are the same for insertion and release. The inner surface is weakly solvophobic. However, the solute properties are different for the two events. Since the unfolded protein possesses large EV and weak solvophobicity, it is driven to be strongly inserted by $-\Phi_S/k_B$ and weakly inserted by $\Phi_E/(k_BT)$, and the net action is insertion. The folded protein is characterized by small EV and solvophilicity with the result that the power of insertion by $-\Phi_S/k_B$ becomes weaker and $\Phi_E/(k_BT)$ dominates. The folded protein is released back to the bulk solvent for preferential solvation. The switch from insertion to release is thus realized. An important point is that $\Phi_E/(k_BT)$ is requisite in release. In TolC, by contrast, the solute properties remain unchanged for insertion and release. To accomplish the release, the vessel inner

surface needs to be solvophobic for a solvophilic solute, whereas it needs to be solvophilic for a solvophobic solute. It turns out that releasing both of the solvophilic and solvophobic solutes is not achievable.

Our basic idea is as follows: Only the entropic component of the PMF possesses the insensitivity to the solute-solvent and vessel inner surface-solvent affinities; and the multidrug efflux can be realized if the entropic component predominates over the energetic one. When the vessel inner surface is neither solvophobic nor solvophilic, the solvents within the vessel cavity and in the bulk offer almost the same environment to any solute with solvophobicity or solvophilicity, and the energetic component becomes much less powerful than the entropic component (i.e., the latter dominates). This can be relevant to TolC whose inner surface possesses a mixture of predominantly nonpolar and isolated electronegative patches.[1] The remaining issue is to explore how to release a solute *entropically*.

In the present study, we calculate the spatial distribution of the PMF between a big sphere and a cylindrical vessel with two open ends immersed in small spheres using the three-dimensional (3D) integral equation theory[9,10,14–17,21–26] combined with rigid-body models in which the constituents interact only through hard-body potentials. The big sphere and small spheres correspond to a solute and solvent, respectively, and the vessel is a model of TolC. To focus our analysis on the entropic component of the PMF, we employ the rigid-body models mentioned above where all of the allowed system configurations share the same energy and the system behavior is purely entropic in origin. Namely, we look at $\Phi/(k_BT)$ possessing only the entropic component: $\Phi/(k_BT) = -\Phi_S/k_B$. Unlike in our earlier works,[14–16] the vessel geometry is made variable after the solute insertion. (For a fixed geometry of the vessel, the solute remains confined within the vessel cavity once it is inserted.) It is demonstrated that release can also be realized by the entropic component of the PMF: The solute is entropically moved from the entrance to the exit by a continuous variation of the vessel geometry. Due to the PMF periodicity of $d_S = 0.28$ nm explained above, even a vessel-geometry variation of this scale leads to a drastic change in the spatial distribution of the PMF, thus enabling the vessel to control the solute motion. The key factor is a time-dependent entropic force acting on a solute, which originates from the solvent-mediated interaction between the solute and the vessel whose geometry is continuously varied and time dependent. Solutes with a wide range of sizes are entropically released using the same vessel-geometry variation. Such rich behavior is observed even in our simplified model neglecting the potentials other than hard-body potentials and polyatomic structures of the vessel and the solute.

A brief report has already been published by us in a Letter,[17] but much more extensive parametric studies are carried out with detailed arguments in the present article. In particular, we show for the first time that solutes with a wide range of sizes can be handled, thus developing a sounder physical basis of the multidrug efflux. The conclusions drawn are fairly general and also applicable to other proteins (or protein complexes) exhibiting the multidrug efflux such as AcrB and ATP-binding cassette (ABC) transporter.[27,28]

II. MODEL AND THEORY

A. Three-dimensional integral equation theory applied to rigid-body models

Though the model, basic equations, numerical solution strategy were described in our earlier brief report,[17] they are reinterpreted here.

In biological systems, the solvent is water characterized by hydrogen bonds. Solute insertion into water, for instance, causes restrictions of translational and rotational freedoms of water molecules. However, the contribution from the translational restriction is much larger: In hydration thermodynamics of a solute, the translational entropy predominates over the rotational entropy.[29,30] In many cases, the translational-entropy effect can be described by modeling water as hard spheres as long as the diameter and number density of the hard-sphere solvent are set at those of water.[31,32] (An exception is found in the elucidation of cold denaturation of a protein[33–35] where the weakening of the entropic effect at low temperatures plays essential roles and a suitable molecular model is necessitated for water.) We note that the hydrogen bonding allows water to exist as a dense liquid despite its quite a small molecular size, leading to an exceptionally large entropic effect.

We consider rigid-body models in which the constituents interact only through hard-body potentials: a big hard vessel and a big hard sphere immersed at infinite dilution in small hard spheres with diameter d_S forming the solvent. The big sphere corresponds to a solute and its diameter is denoted by d_B. The initial geometry of the vessel is shown in Fig. 2(a). After the solute insertion, the vessel geometry is varied for

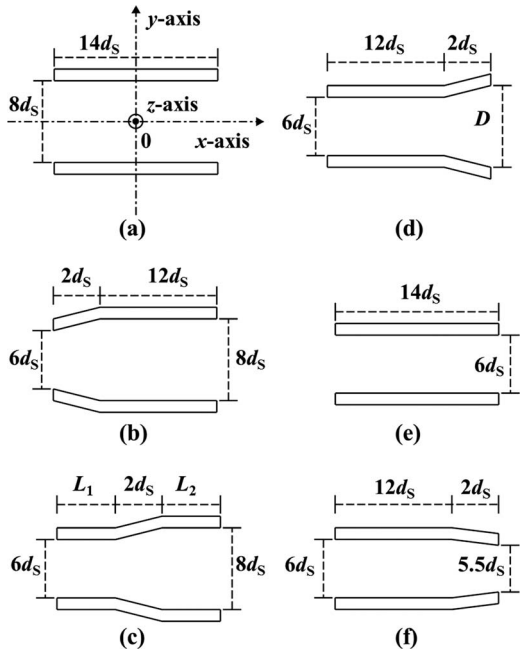

FIG. 2. Variation of vessel geometry: (a)→(b)→(c)→(d)→(e)→(f). The geometry in (a) is a cylinder with inner diameter $8d_S$, length $14d_S$, and thickness d_S (d_S is the molecular diameter of the solvent). The coordinate system is chosen as illustrated here. In the geometry in (d), $D = 8d_S$. D is reduced as (d)→(e)→(f). The cross section of $z = 0$ is shown for each geometry. Though the geometry variation is illustrated in a stepwise manner, it is made *continuously*.

the solute release as explained in Figs. 2(b)–2(f). The Cartesian coordinate system is chosen as illustrated in Fig. 2(a). The cross section of $z = 0$ is shown for each geometry. More details are described in Sec. II B.

The vessel with a prescribed geometry is considered. First, the solvent-solvent correlation functions are calculated using the radial-symmetric (RS) hypernetted-chain (HNC) theory for spherical particles.[36] Second, the vessel-solvent correlation functions are calculated by means of the 3D integral equation theory described below. This theory[9,10,14–17,21–26] and the density functional theory[37–40] have been applied to a variety of important problems in biophysics and colloidal science with the emphasis on the entropic force[41,42] induced between big, spherical and nonspherical bodies immersed in small spheres.[9,10,14–17,23,25,26,37–40] Third, the solute-solvent correlation functions are calculated using the RS-HNC theory for spherical particles.[36] The PMF between the vessel and the solute is then calculated by assuming that the solvent particles are always in equilibrium with each configuration of the vessel-solute pair.

The Ornstein-Zernike (OZ) equation in the Fourier space is expressed by[9,10,14–17,21–26]

$$W_{1S}(k_x, k_y, k_z) = \rho_S C_{1S}(k_x, k_y, k_z) H_{SS}(k). \quad (1)$$

This is coupled with the HNC closure equation written as[9,10,14–17,21–26]

$$c_{1S}(x, y, z) = \exp\{-u_{1S}(x, y, z)/(k_B T)\} \exp\{w_{1S}(x, y, z)\} - w_{1S}(x, y, z) - 1. \quad (2)$$

In these equations, the subscripts "1" and "S" denote the vessel and the solvent, respectively, $w = h - c$, c is the direct correlation function, h is the total correlation function, u is the potential, and ρ_S is the bulk density. The molecular diameter d_S is set at the value of water, 0.28 nm. The reduced number density $\rho_S d_S^3$ is taken to be the value of water at 298 K and 1 atm, 0.7317. C, H, and W represent the Fourier transforms of c, h, and w, respectively. $H_{SS}(k)$ ($k^2 = k_x^2 + k_y^2 + k_z^2$) calculated using the RS-HNC theory for spherical particles[36] is part of the input data. We emphasize that the OZ equation is *exact*.[43] It has been stated that the OZ equation includes serious approximations in a publication,[38] but this statement is incorrect. On the other hand, the bridge function is neglected in the HNC closure equation. However, it has been corroborated that the 3D-OZ-HNC theory gives quantitatively reliable results.[10]

The numerical procedure is briefly summarized as follows: (1) $u_{1S}(x, y, z)$ is calculated at each 3D grid point, (2) $w_{1S}(x, y, z)$ is initialized to zero, (3) $c_{1S}(x, y, z)$ is calculated from Eq. (2), and $c_{1S}(x, y, z)$ is transformed to $C_{1S}(k_x, k_y, k_z)$ using the 3D fast Fourier transform (3D-FFT), (4) $W_{1S}(k_x, k_y, k_z)$ is calculated from Eq. (1), and $W_{1S}(k_x, k_y, k_z)$ is inverted to $w_{1S}(x, y, z)$ using the 3D-FFT, and (5) steps (3) and (4) are repeated until the input and output functions for $w_{1S}(x, y, z)$ become identical within convergence tolerance. On grid points where a solvent particle and the solute overlap, $\exp\{-u_{1S}(x, y, z)/(k_B T)\}$ is zero. On those where a solvent particle is in contact with the solute, it is set at 0.5, and otherwise it is unity. The grid spacing (Δx, Δy, and Δz) is set at $0.1 d_S$, and the grid resolution ($N_x \times N_y \times N_z$) is $256 \times 256 \times 256$. It has been confirmed that the spacing is sufficiently small and the box size ($N_x \Delta x$, $N_y \Delta y$, $N_z \Delta z$) is large enough for the correlation functions at the box surfaces to be essentially zero.

The Fourier transform of the vessel-solvent direct correlation function denoted by $C_{1S}(k_x, k_y, k_z)$ is calculated in accordance with the procedure described above. The Fourier transforms of the solute-solvent total correlation function denoted by $H_{2S}(k)$ (the subscript "2" denotes the solute) is calculated using the RS-HNC theory for spherical particles where $H_{SS}(k)$ is part of the input data. The PMF between the vessel and the solute, $\Phi_{12}(x, y, z)$, is then obtained from

$$\Phi_{12}(x, y, z)/(k_B T) = u_{12}(x, y, z)/(k_B T) - w_{12}(x, y, z), \quad (3)$$

where $w_{12}(x, y, z)$ is calculated by inverting $W_{12}(k_x, k_y, k_z)$ given by

$$W_{12}(k_x, k_y, k_z) = \rho_S C_{1S}(k_x, k_y, k_z) H_{2S}(k). \quad (4)$$

The two equations,[16,26]

$$\Phi_{12}(x, y, z) = F(x, y, z) - F_\infty \quad (5)$$

and

$$g_{12}(x, y, z) = \exp\{-\Phi_{12}(x, y, z)/(k_B T)\}, \; g_{12,\infty} = 1, \quad (6)$$

allow us to understand the physical meaning of $\Phi_{12}(x, y, z)$. Here, $F(x, y, z)$ is the free energy of small spheres in the case where the solute center is at the position (x, y, z), and $g_{12}(x, y, z)$ is the pair distribution function. The subscript "∞" denotes the value in the case where the solute is infinitely separated from the vessel. For rigid-body models, the behavior of $\Phi_{12}(x, y, z)$ is purely entropic in origin. Due to the microscopic structure of small spheres formed within the domain confined by the solute and the vessel, $\Phi_{12}(x, y, z)$ exhibits a complex spatial distribution. A great advantage of the 3D integral equation theory is that the values of Φ_{12} on all the grid points are obtained from only a single calculation, which is not inherent in the usual computer simulation (e.g., a molecular dynamics (MD) simulation).

B. Variation of vessel geometry

We emphasize that the vessel-geometry variation is made *continuously* though it is represented in a stepwise manner in Fig. 2. Figure 2(a) shows the initial geometry of the vessel, a cylinder with inner diameter $8d_S$, length $14d_S$, and thickness d_S. These dimensions roughly mimic those of TolC except that the length is set at a much shorter value (the length of TolC in the real system is $\sim 50 d_S$).[44] This is because all we need in the present study is a length which is sufficiently longer than the diameter of the solute d_B set at $2d_S - 5d_S$. The left and right ends of the cylindrical vessel are the entrance and the exit, respectively. The inner diameter at the entrance is first reduced to $6d_S$ (Fig. 2(b)). L_1 and L_2, lengths of the portions with inner diameter $6d_S$ and $8d_S$, respectively, are gradually increased and decreased, respectively (Fig. 2(c)). Since the length of the tapering portion is set at $2d_S$, $L_1 + L_2 = 12d_S$. The inner diameter at the exit D is gradually reduced after the geometry with $D = 8d_S$ shown in Fig. 2(d)

is reached. In the case of $D = 6d_S$, the inner diameter uniformly becomes $6d_S$ (Fig. 2(e)). As the final geometry, D is made smaller than $6d_S$ ($D = 5.5d_S$ in Fig. 2(f)). Hereafter, the vessel geometries shown in Figs. 2(a)–2(f) are referred to as vessel geometries (a), (b), (c), (d), (e), and (f), respectively.

In AcrA/AcrB/TolC, the proton motive force causes structural changes of AcrB, which are transmitted to TolC through AcrA.[5,6,8] This action may lead to a continuous vessel-geometry variation of TolC. On the other hand, a recent MD simulation study[44] has suggested that TolC can vary its geometric characteristics by itself: They have observed a peristaltic motion of the periplasmic domain and closing and opening for both of the periplasmic and extracellular mouths. This observation is consistent with the geometry variation illustrated in Fig. 2. We start with the geometry of Fig. 2(a) where the left end corresponding to the periplasmic mouth is opened. In the geometry of Fig. 2(f), the right end corresponding to the extracellular mouth begins to change its geometry toward closing. Of course, details of the geometry variation in the real system during the insertion/release process are not known. However, our conclusions are independent of the details as discussed in Sec. III E. What we emphasize in the present study is that release as well as insertion of solutes with a wide range of sizes can be achieved entropically and that a continuous vessel-geometry variation plays essential roles.

III. RESULTS AND DISCUSSION

A. Entropic potential for vessel geometry (a) in Fig. 2

Hereafter, the PMF scaled by k_BT between the vessel and the solute are denoted simply by $-\Phi_S/k_B$ because the equation, $\Phi/(k_BT) = -\Phi_S/k_B$, holds for our model system. We refer to $-T\Phi_S$ as "entropic potential." Unless otherwise mentioned, the solute size d_B is set at md_S ($m = 2, 3, 4, 5$).

Figure 3 shows the distributions of $-\Phi_S/k_B$ on the cross section of $z = 0$ for vessel geometry (a) (see Fig. 2(a)) for the four values of d_B. As the color approaches dark blue, $-\Phi_S/k_B$ and the free energy of the solvent become lower and the solute is more stabilized there. As the color approaches dark red, they become higher and the solute is more destabilized there. The center of the big sphere cannot enter the domain drawn in white. The stripe pattern of the entropic potential formed along the y-axis can physically be interpreted as follows. When the separation between the nearest solute and vessel inner surfaces, which is denoted by η, is not sufficiently close to nd_S ($n = 0, 1, 2, \ldots$), spaces unavailable to the translational displacement of solvent molecules appear as indicated in Fig. 4(a). By contrast, in cases of $\eta \sim nd_S$, such unfavorable spaces do not appear and the solvent particles can efficiently be packed within the domain confined between two surfaces as illustrated in Fig. 4(b). The configuration in Fig. 4(a) is entropically unfavorable, while that in Fig. 4(b) is entropically favorable, leading to the stripe pattern formed along the y-axis. The inner diameter of vessel geometry (a) is $8d_S$. The entropic potential in the central region around $y = 0$ is negative when $(8d_S - d_B)/d_S$ is even (i.e., $d_B = 2d_S$ or $4d_S$), whereas it is positive when $(8d_S - d_B)/d_S$ is odd (i.e., $d_B = 3d_S$ or $5d_S$), as observed in Fig. 3. The amplitude of the stripe pattern formed along the y-axis becomes progressively larger as the solute size increases.

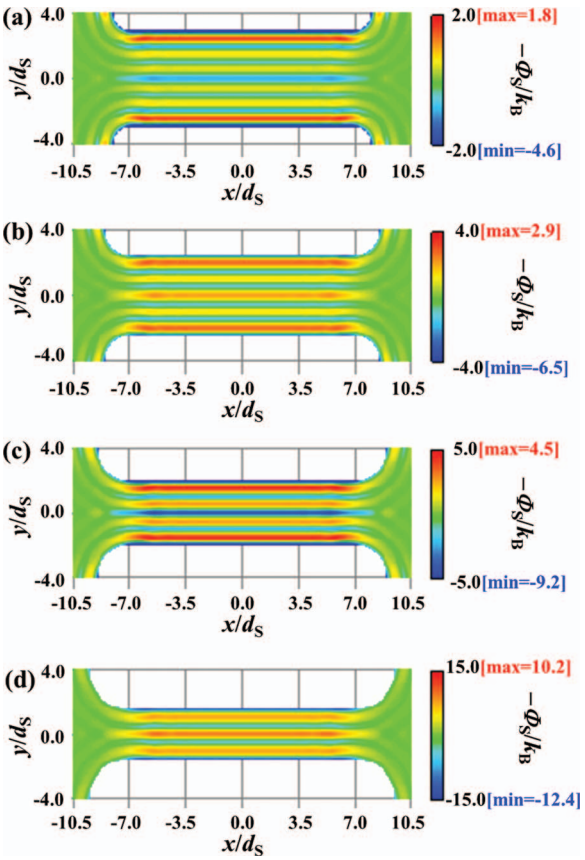

FIG. 3. Distributions of $-\Phi_S/k_B$ on the cross section of $z = 0$ for the initial vessel geometry illustrated in Fig. 2(a) for the solutes with $d_B = 2d_S$ (a), $d_B = 3d_S$ (b), $d_B = 4d_S$ (c), and $d_B = 5d_S$ (d). $-\Phi_S/k_B$ becomes lower as the color approaches dark blue, and it becomes higher as the color approaches dark red ("max" and "min" represent the maximum and minimum values, respectively). The center of the big sphere cannot enter the domain drawn in white.

It was experimentally shown for the entropic interaction between large spheres immersed in small spheres that a free-energy barrier well exceeding k_BT cannot readily be overcome and that with the barrier of $\sim 2k_BT$ the large spheres come

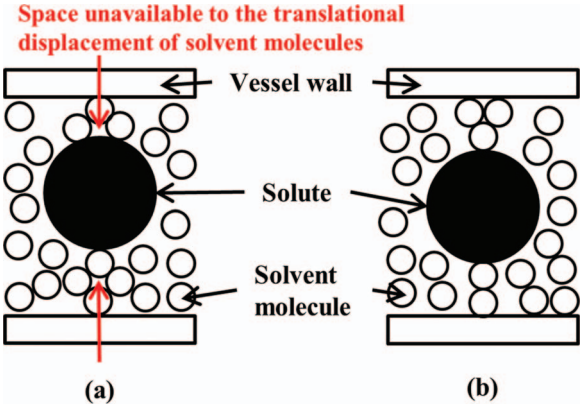

FIG. 4. Cartoons illustrating how the stripe pattern of the entropic potential shown in Fig. 2(a) is formed along the y-axis. (a) Separation between the nearest solute and vessel inner surfaces, which is denoted by η, is not sufficiently close to nd_S ($n = 0, 1, 2, \ldots$). (b) In the case of $\eta \sim nd_S$.

together only rarely.[45] The best way of discussing a barrier is to analyze the dynamic behavior of the solute by solving the Fokker-Planck equation. Such a detailed analysis, which provides us with useful information on the time required for overcoming it, is an issue to be pursued in the near future. In the present study, we discuss a barrier in reference to the experimental observation mentioned above. (As argued below, the time required for overcoming the barrier in the final stage of the solute release at the exit can be an important quantity: It is better to make this time as short as possible by keeping the barrier as low as possible. See the fourth and fifth paragraphs in "CONCLUSIONS" for a more detailed discussion.)

As observed in Fig. 3, the solute is most likely to be inserted into the central region around $y = 0$ for $d_B = 2d_S$ or $4d_S$ and into the region next to the central one around $y/d_S = \pm 0.5$ for $d_B = 3d_S$ or $5d_S$ (these regions are referred to as the most stable regions). However, for all the solute sizes tested there is a possibility that the solute is inserted into a different region with negative $-\Phi_S/k_B$ due to the presence of a trajectory possessing a sufficiently low barrier. As shown in our earlier works,[14–16] a modification of the vessel geometry (e.g., truncation of the edge at the entrance) increases the barriers in a trajectory in the region $x/d_S < -7$ along which the solute can touch the vessel and may enable the solute to be inserted into the most stable region with higher probability. In any case, we postulate that the solute is inserted into the most stable region for each solute size. This postulation is justified because in the real system AcrB interacting with TolC at its entrance sends the solute to the central position within the vessel cavity.

The profiles of $-\Phi_S/k_B$ along "$y = 0$ and $z = 0$" (i.e., the x-axis) are shown in Fig. 5(a) for $d_B = 2d_S$ and $4d_S$. Those along "$y/d_S = \pm 0.5$ and $z = 0$" are presented in Fig. 5(b) for $d_B = 3d_S$ and $5d_S$. The dotted line indicates the position near the entrance where $-\Phi_S/k_B$ takes the lowest value. The position is located at $x/d_S = -5.5$ in Fig. 5(a) and at $x/d_S = -5.7$ in Fig. 5(b). Figure 6 shows the profiles of $-\Phi_S/k_B$ in the radial direction along "$x/d_S = -5.5$ and $z = 0$" for $d_B = 2d_S$ and $4d_S$ together with those along "$x/d_S = -5.7$ and $z = 0$" for $d_B = 3d_S$ and $5d_S$. The open circle indicates the position where the solute is stabilized with the highest probability right after the solute insertion. If the vessel geometry underwent no change, the solutes with $d_B = 4d_S$ and $5d_S$ would remain confined within the region of $-6 < x/d_S < 6$ (see Fig. 5). A problem is that the solutes with $d_B = 2d_S$ and $3d_S$ may go in the left direction by overcoming the barriers of $\sim k_B T$. Moreover, the solute with $d_B = 2d_S$ may move in the radial direction without difficulty (see Fig. 6). These unfavorable motions of the smaller solutes can be prevented by the variation in the vessel geometry which is made as soon as the solute is inserted into the most stable region for each solute size. More details are discussed in Sec. III B.

B. Entropic potentials for vessel geometries (b), (c), and (d) in Fig. 2

For the solute with $d_B = 2d_S$, the distributions of $-\Phi_S/k_B$ on the cross section of $z = 0$ for vessel geometries (b), (c), and (d) (see Figs. 2(b)–2(d)) are shown in Figs. 7(a)–7(c), respectively. Those for the solutes with $d_B = 3d_S$, $4d_S$, and $5d_S$ are

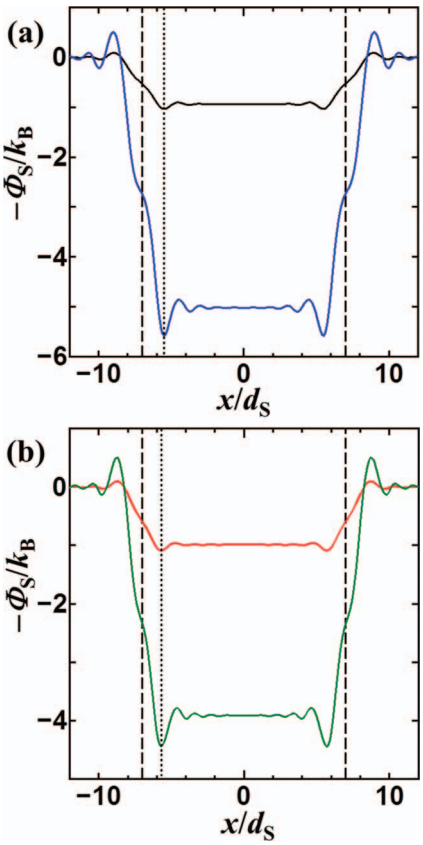

FIG. 5. (a) Profiles of $-\Phi_S/k_B$ along "$y = 0$ and $z = 0$" for $d_B = 2d_S$ (black) and $4d_S$ (blue). (b) Those along "$y/d_S = \pm 0.5$ and $z = 0$" for $d_B = 3d_S$ (red) and $5d_S$ (green). The two broken lines in each plot represent positions of the vessel ends, $x/d_S = \pm 7$. The dotted line indicates the position near the entrance where $-\Phi_S/k_B$ takes the lowest value.

presented in Figs. 8–10, respectively. In vessel geometry (c), $L_1 = L_2 = 6d_S$. The open circle indicates the position where the entropic potential is locally minimum. For the portion of length L_1 as well as for that of length L_2 (see Fig. 2(c)), the entropic potential in the central region around $y = 0$ is negative when $(8d_S - d_B)/d_S$ is even (i.e., $d_B = 2d_S$ or $4d_S$), whereas it is positive when $(8d_S - d_B)/d_S$ is odd (i.e., $d_B = 3d_S$ or $5d_S$).

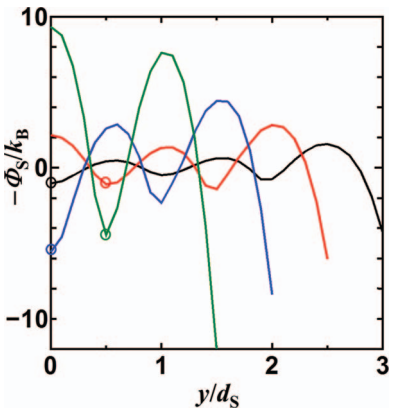

FIG. 6. Profiles of $-\Phi_S/k_B$ in the radial direction along "$x/d_S = -5.5$ and $z = 0$" for $d_B = 2d_S$ (black) and $4d_S$ (blue), and those along "$x/d_S = -5.7$ and $z = 0$" for $d_B = 3d_S$ (red) and $5d_S$ (green). The open circle indicates the position where the solute is stabilized with the highest probability right after the solute insertion.

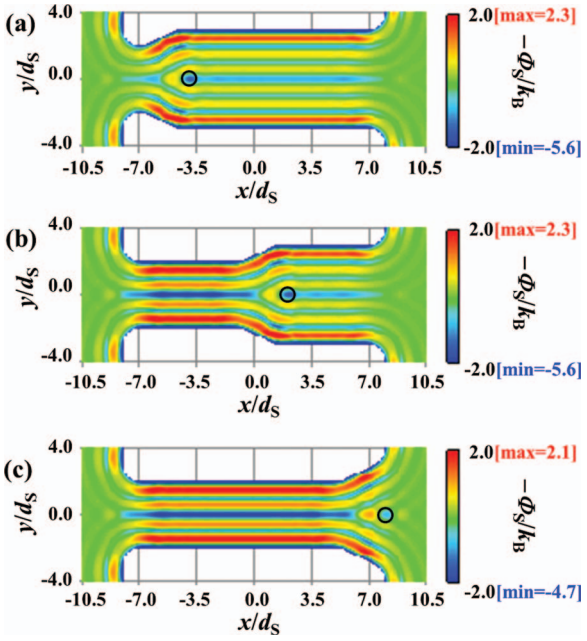

FIG. 7. Distributions of $-\Phi_S/k_B$ on the cross section of $z = 0$ for vessel geometries (b), (c), and (d) illustrated in Figs. 2(b)–2(d), respectively. The solute size d_B is $2d_S$. $-\Phi_S/k_B$ becomes lower as the color approaches dark blue, and it becomes higher as the color approaches dark red ("max" and "min" represent the maximum and minimum values, respectively). The open circle indicates the position where the entropic potential is locally minimum.

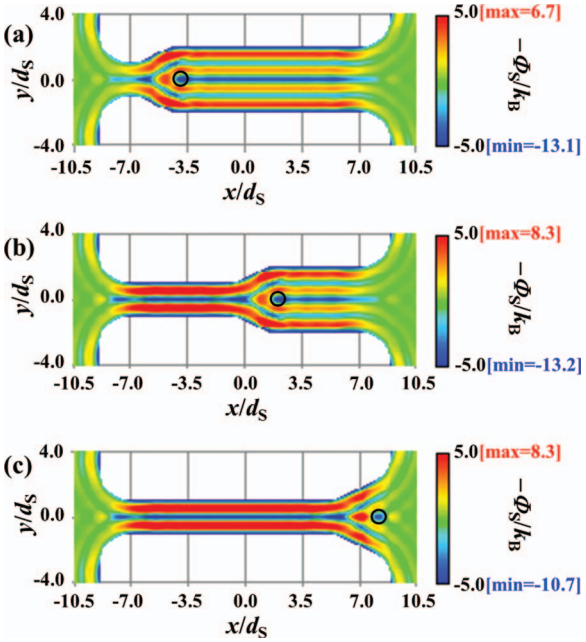

FIG. 9. Distributions of $-\Phi_S/k_B$ on the cross section of $z = 0$ for vessel geometries (b), (c), and (d) illustrated in Figs. 2(b)–2(d), respectively. The solute size d_B is $4d_S$. $-\Phi_S/k_B$ becomes lower as the color approaches dark blue, and it becomes higher as the color approaches dark red ("max" and "min" represent the maximum and minimum values, respectively). The open circle indicates the position where the entropic potential is locally minimum.

Within the intermediate portion (i.e., portion of length $2d_S$) around the x-axis, a small domain with positive $-\Phi_S/k_B$ is formed for $d_B = 2d_S$ or $4d_S$, while that with negative $-\Phi_S/k_B$ is formed for $d_B = 3d_S$ or $5d_S$. Next to the solute on the left side, the potential becomes positive regardless of the solute size. Since L_1 is continuously lengthened as illustrated in Fig. 2, the solutes with all the sizes tested are driven to move in the right direction along the x-axis toward the exit (see Figs. 7–10).

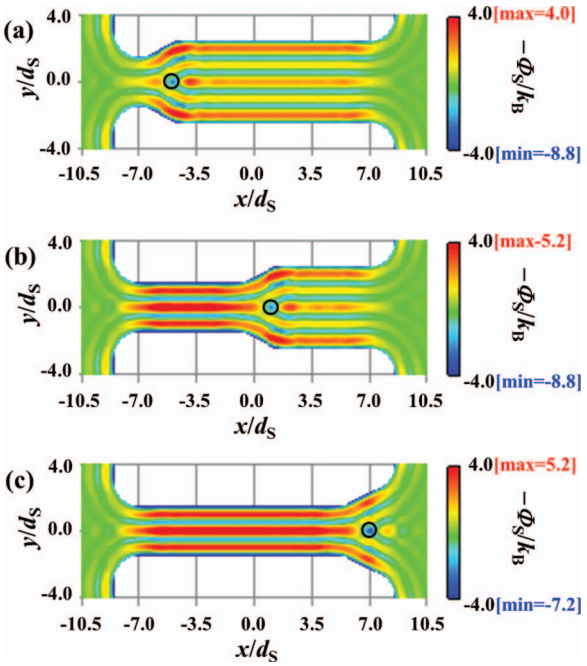

FIG. 8. Distributions of $-\Phi_S/k_B$ on the cross section of $z = 0$ for vessel geometries (b), (c), and (d) illustrated in Figs. 2(b)–2(d), respectively. The solute size d_B is $3d_S$. $-\Phi_S/k_B$ becomes lower as the color approaches dark blue, and it becomes higher as the color approaches dark red ("max" and "min" represent the maximum and minimum values, respectively). The open circle indicates the position where the entropic potential is locally minimum.

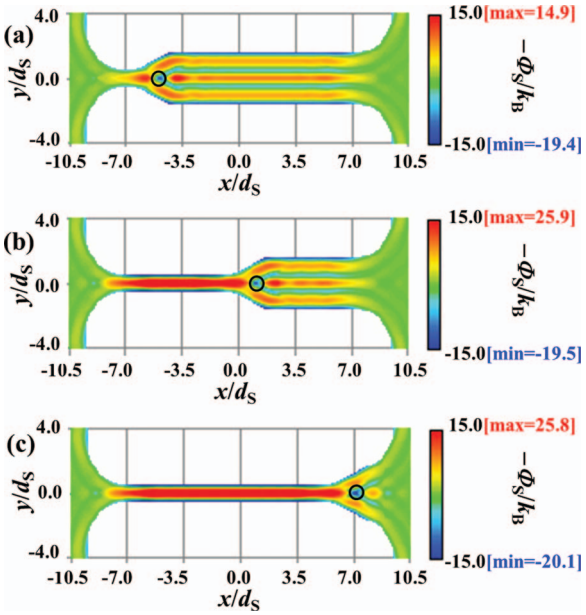

FIG. 10. Distributions of $-\Phi_S/k_B$ on the cross section of $z = 0$ for vessel geometries (b), (c), and (d) illustrated in Figs. 2(b)–2(d), respectively. The solute size d_B is $5d_S$. $-\Phi_S/k_B$ becomes lower as the color approaches dark blue, and it becomes higher as the color approaches dark red ("max" and "min" represent the maximum and minimum values, respectively). The open circle indicates the position where the entropic potential is locally minimum.

A notable point is that the entropic potential does not remain constant: It is time dependent. There are three different time scales: those of the solvent motion, variation in the vessel geometry, and solute motion. The time scale of the solvent motion is doubtlessly the fastest. The solvent is practically in equilibrium with the solute-vessel configuration all the time. Here, we assume that the variation of the vessel geometry (that is, the variation of the entropic potential) is relatively faster than the solute motion. The faster variation of the vessel geometry could be realized by structural changes of AcrB caused by the proton motive force. It follows that an entropic force, which is given as $F_S = -\{\partial(-T\Phi_S)/\partial x\}$, *continuously* acts on the solute in the right direction along the x-axis and continues to accelerate its motion during the variation of the vessel geometry. When vessel geometry (d) is reached, the solute should possess a considerably high velocity. As a consequence, even a barrier well exceeding k_BT can readily be overcome by the solute.

Figure 11(a) shows the entropic forces acting on the solute with $d_B = 2d_S$ in vessel geometry (c). They are for $(L_1, L_2) = (6d_S, 6d_S)$ and for $(L_1, L_2) = (6.1d_S, 5.9d_S)$, respectively. A similar plot is made in Fig. 11(b) for the solute with $d_B = 5d_S$. When the solute is at the location indicated by the dashed-dotted line representing the potential minimum for $(L_1, L_2) = (6d_S, 6d_S)$, the force looking like that for $(L_1, L_2) = (6.1d_S, 5.9d_S)$ is applied to the solute. This is because the solute is always on the left side of (and close to) the location with the potential minimum when the variation of the vessel geometry is relatively faster than the solute motion. The force continuously accelerates the solute motion in the right direction along the x-axis. The maximum value of the force increases remarkably as the solute size becomes larger: For instance, it is approximately 25 times stronger for $d_B = 2d_S$ than for $d_B = 5d_S$.

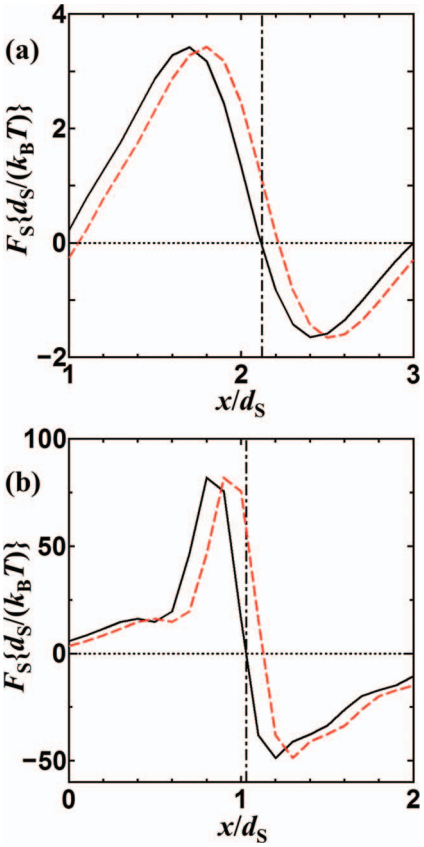

FIG. 11. Entropic forces acting on the solute in vessel geometry (c) illustrated in Fig. 2(c) for $(L_1, L_2) = (6d_S, 6d_S)$ (black and solid) and for $(L_1, L_2) = (6.1d_S, 5.9d_S)$ (red and broken). The solute size d_B is $2d_S$ in (a) and $5d_S$ in (b). The position of the potential minimum for $(L_1, L_2) = (6d_S, 6d_S)$ is indicated by the dashed-dotted line.

C. Entropic potentials for vessel geometries (d), (e), and (f) in Fig. 2

To complete the release of the solute, the inner diameter at the exit D is gradually reduced as illustrated in Figs. 2(d)–2(f). Figure 12(a) shows the profiles of $-\Phi_S/k_B$ along the x-axis for vessel geometries (d) ($D = 8d_S$), (d) with $D = 7d_S$, (e) ($D = 6d_S$), and (f) ($D = 5.5d_S$) for the solute with $d_B = 2d_S$. Those for the solute with $d_B = 5d_S$ are displayed in Fig. 12(b). The open circle indicates the position where the entropic potential is locally minimum. The coordinate, $(x/d_S, y/d_S, z/d_S) = (7, 0, 0)$, corresponds to the position where the right half of the solute is outside the vessel. As D decreases, the solute is driven to move further in the right direction along the

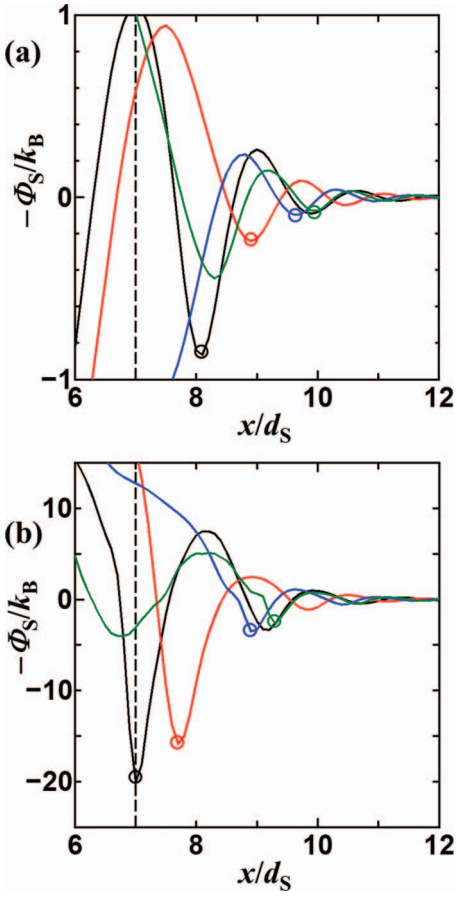

FIG. 12. Profiles of $-\Phi_S/k_B$ along the x-axis for vessel geometries (d) with $D = 8d_S$ (black), (d) with $D = 7d_S$ (red), (e) (blue), and (f) (green). The solute size d_B is $2d_S$ in (a) and $5d_S$ in (b). The open circle indicates the position where the entropic potential is locally minimum. The coordinate, $(x/d_S, y/d_S, z/d_S) = (7, 0, 0)$, corresponds to the position where the right half of the solute is outside the vessel. The broken line in each plot represents position of the right end of the vessel, $x/d_S = 7$.

x-axis and the barrier becomes progressively lower. It should be quite easy for the solute with $d_B = 2d_S$ to overcome the barrier for being released to the bulk, even in vessel geometry (d) ($D = 8d_S$). However, the barriers become higher as the solute size increases. For the solute with $d_B = 5d_S$, though the velocity of the solute in the right direction along the x-axis is expected to be much higher than for the solute with $d_B = 2d_S$, it is not definite if the barriers in vessel geometries (d) ($D = 8d_S$), (d) with $D = 7d_S$, and (e) ($D = 6d_S$) can be overcome. Fortunately, the barrier decreases to $\sim 3.5\, k_B T$ in vessel geometry (f) ($D = 5.5d_S$). This value should be sufficiently low in the light of the very strong entropic force discussed in Sec. III B.

From the above argument, we conclude that solutes with a wide range of sizes can be released to the bulk. The key idea is a continuous variation of the vessel geometry accompanying that of the spatial distribution of the entropic potential. We remark that the solute velocity in the final vessel geometry considered becomes higher as the vessel length increases. In other words, a longer vessel enables the solute to overcome a higher barrier for being released to the bulk. Even a barrier that is considerably higher than $k_B T$ could readily be overcome. The very large value of the length of TolC, $\sim 50d_S$, may play crucially important roles in the solute release.

Within the cylindrical vessel with two open ends (i.e., entrance and exit for the solute), the solute motion is thus directed only toward the right end. Such unidirectional motion cannot be performed by the mere diffusion: The solute release from the right end is achievable only with the probability of 0.5 at most; and the actual probability is significantly lower than 0.5 since the initial position of the solute is in the vicinity of the left end. Even when the left end is closed (it is confined by AcrB in the real system), the probability that the solute remains near the left end is considerably high.

D. Case where solute size differs from integral multiplication of d_S

We consider the solute sizes that differ from the integral multiplication of d_S: Solutes with the 11 sizes, $d_B = 3d_S + 0.1md_S$ ($m = 0-10$), are compared. We find that the stripe pattern observed in Fig. 3 persists even for the solute sizes differing from the integral multiplication of d_S. Figure 13 shows the profiles of $-\Phi_S/k_B$ in the radial direction along "$x/d_S = -p$ and $z = 0$" for $m = 0-10$ ($p = 5.7$, 5.6, 5.8, 6.1, 5.9, 6.0, 6.0, 5.9, 5.7, 5.6, and 5.5, respectively). This figure corresponds exactly to Fig. 6, and the open circle indicates the position where the solute is stabilized with the highest probability right after the solute insertion. It is observed that the barrier to overcome for the solute to reach $y/d_S = 1$ is sufficiently high for all the solute sizes tested. At $y = 0$, $-\Phi_S/k_B$ takes the maximum value for $m = 0-2$ (category 1), whereas it takes the minimum value for $m = 7-10$ (category 2). $-\Phi_S/k_B$ for $m = 3$ behaves like that in category 1 in the sense that the solute rarely comes to the center of $y = 0$. The profiles of $-\Phi_S/k_B$ for $m = 5$ and 6 are qualitatively similar to those in category 2. $-\Phi_S/k_B$ for $m = 4$ ($d_B = 3.4d_S$) exhibits intermediate behavior.

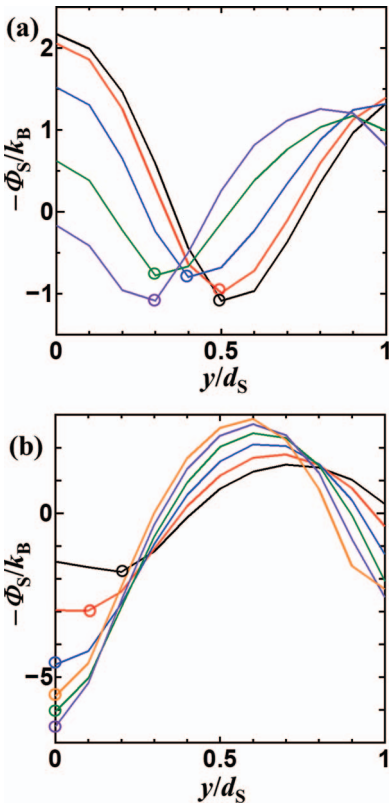

FIG. 13. Profiles of $-\Phi_S/k_B$ in the radial direction for solutes with the 11 different sizes, $d_B = 3d_S + 0.1md_S$ ($m = 0-10$). (a) $m = 0$ (black), $m = 1$ (red), $m = 2$ (blue), $m = 3$ (green), and $m = 4$ (purple). (b) $m = 5$ (black), $m = 6$ (red), $m = 7$ (blue), $m = 8$ (green), $m = 9$ (purple), and $m = 10$ (orange). This figure corresponds exactly to Fig. 6. The open circle indicates the position where the solute is stabilized with the highest probability right after the solute insertion.

The distributions of $-\Phi_S/k_B$ on the cross section of $z = 0$ for vessel geometries (b), (c), and (d) (see Figs. 2(b)–2(d)) are shown for $m = 3$ in Fig. 14. Those for $m = 4$ and 5 are presented in Figs. 15 and 16, respectively. We find that the basic patterns of the distributions for $m = 1-3$ is qualitatively similar to those for $m = 0$ ($d_B = 3d_S$). This sentence is valid when "$m = 1-3$" and "$m = 0$ ($d_B = 3d_S$)" are replaced by "$m = 5-9$" and "$m = 10$ ($d_B = 4d_S$)," respectively. Even for $m = 4$, the potential becomes positive next to the solute on the left side and an entropic force continuously acts on the solute in the right direction along the x-axis and continues to accelerate its motion during the variation of the vessel geometry. The figure corresponding to Fig. 12 is presented for $m = 4$ as Fig. 17. The solute release to the bulk is completed by means of the vessel-geometry variation, (d)→(e)→(f), illustrated in Fig. 2. Similar arguments are possible for the solutes with $d_B = 2d_S + 0.1md_S$ and $d_B = 4d_S + 0.1md_S$ ($m = 0-10$). Thus, solutes with a wide range of sizes can be released *using the same vessel-geometry variation*.

E. Another method of vessel-geometry variation

The method of the vessel-geometry variation achieving the entropic release for solutes with a wide range of sizes is not unique. To demonstrate this, we consider another type of variation illustrated in Fig. 18. Tapering in the diameter from

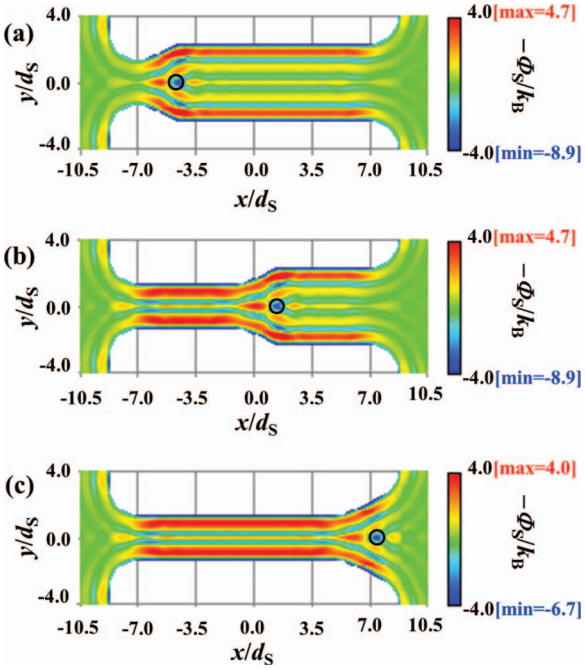

FIG. 14. Distributions of $-\Phi_S/k_B$ on the cross section of $z = 0$ for vessel geometries (b), (c), and (d) (see 2(b)–2(d)) for the solute with $d_B = 3.3d_S$. $-\Phi_S/k_B$ becomes lower as the color approaches dark blue, and it becomes higher as the color approaches dark red ("max" and "min" represent the maximum and minimum values, respectively). The open circle indicates the position where the entropic potential is locally minimum. This figure is to be compared with Figs. 8 and 9.

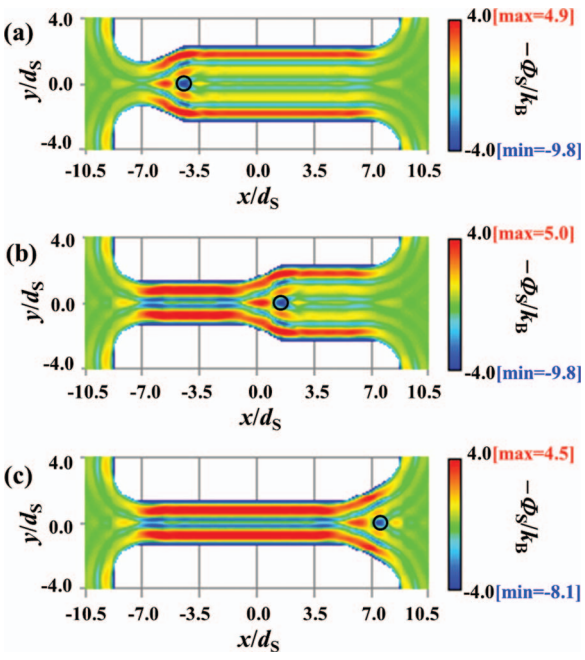

FIG. 15. Distributions of $-\Phi_S/k_B$ on the cross section of $z = 0$ for vessel geometries (b), (c), and (d) (see Figs. 2(b)–2(d)) for the solute with $d_B = 3.4d_S$. $-\Phi_S/k_B$ becomes lower as the color approaches dark blue, and it becomes higher as the color approaches dark red ("max" and "min" represent the maximum and minimum values, respectively). The open circle indicates the position where the entropic potential is locally minimum. This figure is to be compared with Figs. 8 and 9.

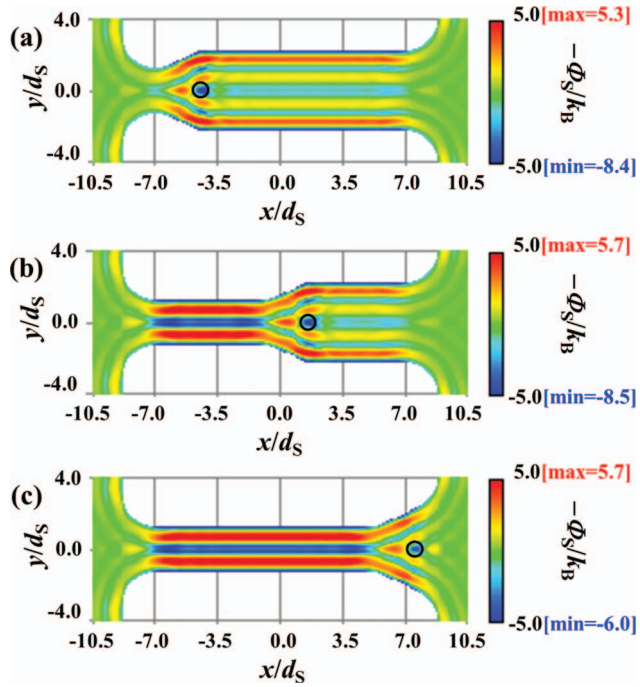

FIG. 16. Distributions of $-\Phi_S/k_B$ on the cross section of $z = 0$ for vessel geometries (b), (c), and (d) (see Figs. 2(b)–2(d)) for the solute with $d_B = 3.5d_S$. $-\Phi_S/k_B$ becomes lower as the color approaches dark blue, and it becomes higher as the color approaches dark red ("max" and "min" represent the maximum and minimum values, respectively). The open circle indicates the position where the entropic potential is locally minimum. This figure is to be compared with Figs. 8 and 9.

$8d_S$ to $6d_S$ is applied only to a small portion of the vessel, and the portion is continuously moved in the right direction toward the exit. Figure 19 shows the distributions of $-\Phi_S/k_B$ on the cross section of $z = 0$ for vessel geometries (b), (c) with $L_1 = L_2 = 5d_S$, (d), and (e) (see Fig. 18) for the solute with $d_B = 3d_S$. The open circle indicates the position where the entropic potential is locally minimum. Those for the solute with $d_B = 4d_S$ are displayed in Fig. 20. An entropic force continuously acts on the solute in the right direction along the x-axis and continues to accelerate its motion during the

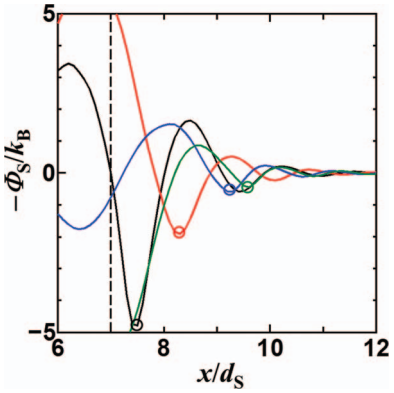

FIG. 17. Plot for the solute with $d_B = 3.4d_S$ corresponding to Fig. 12. The open circle indicates the position where the entropic potential is locally minimum. The coordinate, $(x/d_S, y/d_S, z/d_S) = (7, 0, 0)$, corresponds to the position where the right half of the solute is outside the vessel. The broken line in each plot represents position of the right end of the vessel, $x/d_S = 7$.

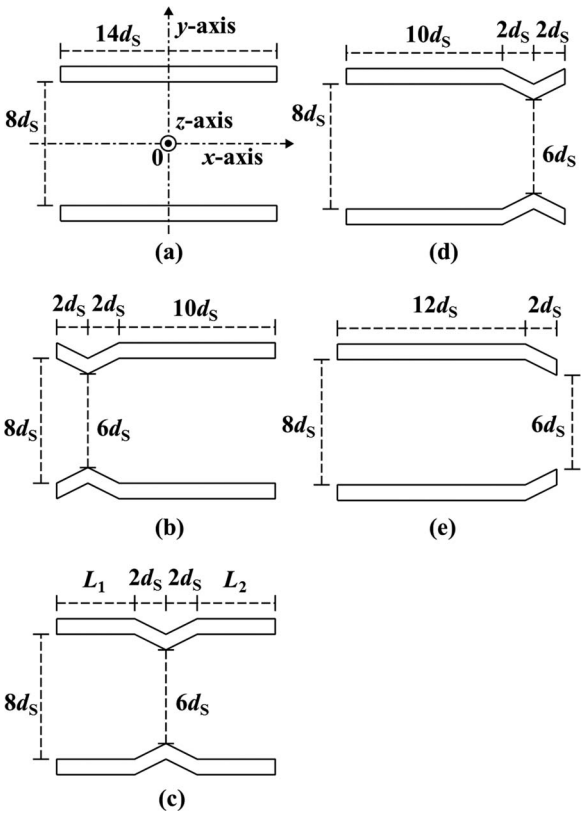

FIG. 18. Variation of vessel geometry: (a)→(b)→(c)→(d)→(e). The geometry in (a) is exactly the same as that in Fig. 2. The coordinate system is chosen as illustrated here. L_1 and L_2 are gradually increased and decreased, respectively. The cross section of $z = 0$ is shown for each geometry. Though the geometry variation is illustrated in a stepwise manner, it is made *continuously*.

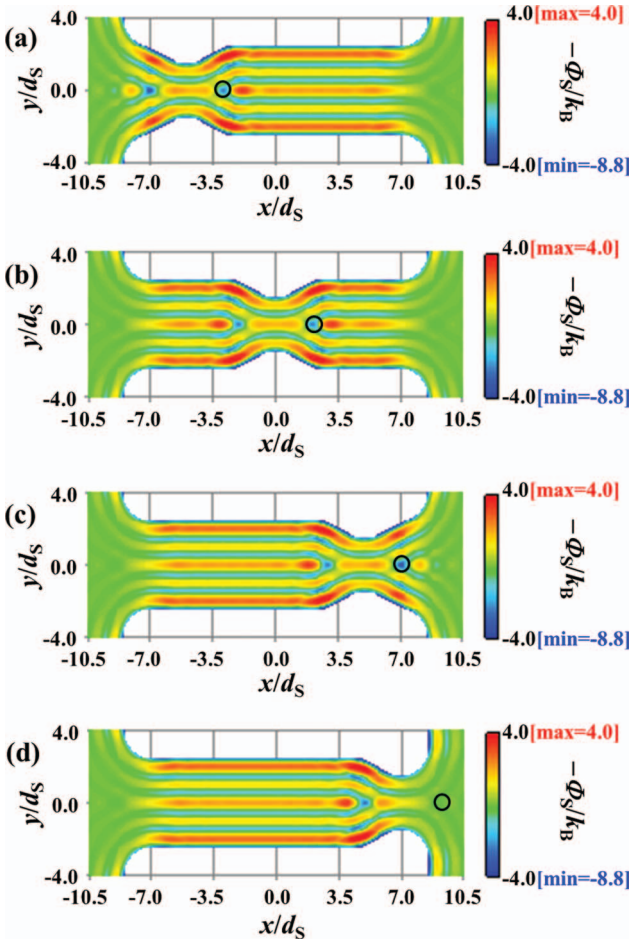

FIG. 19. Distributions of $-\Phi_S/k_B$ on the cross section of $z = 0$ for vessel geometries (b), (c) with $L_1 = L_2 = 5d_S$, (d), and (e) illustrated in Fig. 18. The solute size d_B is $3d_S$. $-\Phi_S/k_B$ becomes lower as the color approaches dark blue, and it becomes higher as the color approaches dark red ("max" and "min" represent the maximum and minimum values, respectively). The open circle indicates the position where the entropic potential is locally minimum.

variation of the vessel geometry. The solute is released to the bulk without difficulty.

We have thus obtained qualitatively the same results for the vessel-geometry variations illustrated in Figs. 2 and 18. A vessel in the real system is expected to exhibit a more complex variation. However, the geometric properties play essential roles and should appropriately be designed just for the portion around the position where the entropic force acts on the solute. The geometric variation for the other portions can be different from that assumed in the present study.

F. Applicability of results obtained to AcrB and ABC transporter

The principal results obtained are as follows: The entropic release of the solute is not feasible as long as the vessel geometry is fixed; it can be accomplished by a continuous variation of the vessel geometry; and solutes with a wide range of sizes can be handled. Namely, a time-dependent entropic force continuing to accelerate the solute motion in the axial direction toward the exit is the key to the multidrug efflux. These results, which are obtained using simple model calculations, seem to be fairly general and applicable to other types of efflux transporters. In the ABC transporter[27,28] with the inward-facing structure and in AcrB[1–8] with the structure drawn in blue in Fig. 1, a solute can spontaneously be inserted into a cavity within the transporter or AcrB. In the transporter, after the solute insertion, the inward-facing structure is gradually changed to the outward-facing one, performing the switch from insertion to release. Similarly, in AcrB the solute release is promoted by a gradual variation from the structure drawn in blue to that drawn in red (see Fig. 1). Our view thus suggested concerning the insertion/release process for AcrB is substantially different from the one relying on the mere diffusion which is unable to perform the unidirectional solute motion.

In AcrB the variation of the structure (i.e., the geometry) is induced by the proton motive force,[1–8] while in ABC transporter it is controlled by the cycle comprising the binding of adenosine triphosphate (ATP), hydrolysis of ATP, and dissociation of Pi and adenosine diphosphate (ADP).[27,28] Despite this difference, these two protein complexes share the feature that the structure is continuously changed to carry out the switch from insertion to release for the solute.

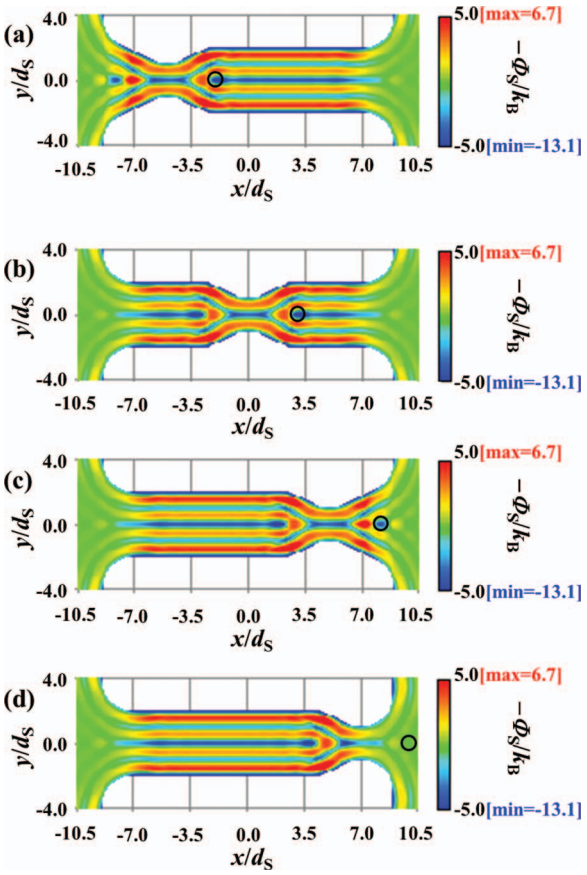

FIG. 20. Distributions of $-\Phi_S/k_B$ on the cross section of $z = 0$ for vessel geometries (b), (c) with $L_1 = L_2 = 5d_S$, (d), and (e) illustrated in Fig. 18. The solute size d_B is $4d_S$. $-\Phi_S/k_B$ becomes lower as the color approaches dark blue, and it becomes higher as the color approaches dark red ("max" and "min" represent the maximum and minimum values, respectively). The open circle indicates the position where the entropic potential is locally minimum.

IV. CONCLUSIONS

We have investigated insertion and release of a solute into and from a cylindrical vessel possessing an entrance at one end and an exit at the other end for the solute. This model vessel mimics TolC, an important component of the multidrug efflux transporter, AcrA/AcrB/TolC.[44] The spatial distribution of the solute-vessel PMF formed by the solvent is calculated using the three-dimensional integral equation theory[9,10,14–17,21–26] combined with rigid-body models in which the constituents interact only through hard-body potentials. With such models, all of the allowed system configurations share the same energy, and the system behavior is purely entropic in origin. It has been demonstrated that the two opposite events, insertion and release, can be driven solely by the entropic effect arising not from the electrostatic and van der Waals interactions for solute-vessel, solute-solvent, solvent-vessel, and solvent-solvent pairs but from the translational displacement of solvent molecules.

A principal aim of the present study is to develop a novel physical picture of the multidrug efflux[6–8] implying that solutes such as drug molecules with diverse properties (i.e., solvophobic and solvophilic solutes with a wide range of sizes) can be handled. The insertion/release process can be described in terms of the PMF consisting of the energetic and entropic components. The energetic component is strongly dependent on the solute-solvent and vessel inner surface-solvent affinities, whereas the entropic component is rather insensitive to them. The basis of our physical picture is that the multidrug efflux can be assured under a condition where the entropic component dominates. This condition is satisfied when the inner surface of the vessel is neither solvophobic nor solvophilic. As long as the vessel geometry is fixed, however, the entropic component does not work for release. A finding is that a solute which has been inserted can also be released entropically using a continuous variation of the vessel geometry. Two typical examples of the variation are illustrated in Figs. 2 and 18. The variation is never unrealistic for the following reasons: The proton motive force causes structural changes of AcrB, they are transmitted to TolC through AcrA,[5,6,8] possibly leading to a continuous vessel-geometry variation of TolC; and a recent molecular dynamics simulation study[44] has suggested that TolC can vary its geometric characteristics even by itself (an observed variation is a peristaltic motion of the periplasmic domain).

The variation of the vessel geometry is initiated as soon as the solute is inserted into the vessel at its entrance. In the real system, the solute insertion is made with the aid of AcrB: AcrB interacting with TolC sends the solute to the central position within the vessel cavity of TolC. The manner of the vessel-geometry variation proposed in the present study generates a time-dependent entropic force. There are three different time scales: those of the solvent motion, variation in the vessel geometry, and solute motion. The time scale of the solvent motion is the fastest, and the solvent is practically in equilibrium with the solute-vessel configuration all the time. We assume that the variation of the vessel geometry (that is, the variation of the entropic potential) is relatively faster than the solute motion. The faster variation of the vessel geometry could be realized by structural changes of AcrB caused by the proton motive force. The time-dependent entropic force then continues to accelerate the solute motion in the axial direction toward the exit. A larger solute is subjected to a stronger force. The solute velocity at the exit becomes higher as the solute size or the vessel length increases. Solutes with a wide range of sizes can be released using the same manner of the variation. It is quite interesting and important that such rich behavior is observed in the very simple model system adopted in the present study.

Once a solute is sent from AcrB to the central position within the TolC cavity, the solute must be ejected to the external medium through the exit before the next solute is sent. Namely, the ejection of every solute needs to be finished with sufficient rapidness. This requirement can be met with much more certainty when the solute motion is directed only toward the exit. This unidirectional motion is assured by the time-dependent entropic force arising from the vessel-geometry variation proposed in the present study. Our physical picture of the multidrug efflux is clearly distinguished from the previously reported one[4,5,12] assuming the existence of multifunctional ligand-binding sites which recognize various types of solutes and relying on the mere diffusion (i.e., the diffusion in the presence of no particular potential field) by which the unidirectional solute motion is not realized. In earlier works,[9–11]

we showed that the solvent entropy plays crucially important roles in the high selectivity pertaining to the receptor-ligand binding. Interestingly, it is also true in the multidrug efflux which is in marked contrast with the high selectivity.

To complement the physical picture of the multidrug efflux, we need to analyze dynamic aspects of the entropic release by solving the Fokker-Planck equation in the presence of a time-dependent force field calculated in the present study. The time required for overcoming the barrier in the final stage of the solute release at the exit is an important quantity. However, it is to be argued in the light of the interval between the two times when a solute and the next solute are sent from AcrB to the central position within the TolC cavity at the entrance. Even if the former time is shorter than the interval, the vessel-geometry variation should still be required. This is because the solute cannot always arrive at the exit in time without its unidirectional motion toward the exit: The long length of TolC ($\sim 50 d_S$) is a noticeable factor. When the vessel-geometry variation is applied, the long length may inversely play crucial roles in the solute release as discussed in Sec. III C. (The interval mentioned above is unknown and to be measured in future experimental and theoretical works.)

The details of the polyatomic structures of the vessel and/or the solute are also essential factors whose effects are to be examined. We remark that our physical picture is fairly general and also applicable to AcrB and ABC transporter[27,28] as discussed in Sec. III F, pending detailed analyses. It is challenging to investigate the sequential structural change exhibited by each protomer of AcrB among three states in which a drug insertion, binding, and release take place.[5,6,8] We have recently developed a novel physical picture[46–48] for F_1-ATPase in which the $\alpha_3\beta_3$ complex always tries to form three regions which are tightly packed, moderately packed, and loosely packed, respectively, and these regions are cyclically exchanged. The inhomogeneous packing structure and the cyclic exchange are attributed to the maintenance of the maximal solvent entropy. This picture, which is consistent with the experimental observations for F_1-ATPase without the γ-subunit,[49] may also be relevant to the sequential structural change in AcrB. The most important matter is treating the solvent as an ensemble of particles with finite sizes to account for the imperative solvent-entropy effect (this has often been neglected as in a recent simulation study[50]). Works along these lines are in progress in our group.

ACKNOWLEDGMENTS

This work was supported by Grant-in-Aid for Scientific Research on Innovative Areas (No. 20118004) and that on (B) (No. 25291035) from the Ministry of Education, Culture, Sports, Science and Technology of Japan (M. Kinoshita), by Kyoto University Global Center of Excellence of Energy Science (H. Mishima), and by Grant-in-Aid for JSPS (Japan Society for the Promotion of Science) fellows (H. Oshima, S. Yasuda, and K. Amano).

[1] V. Koronakis, A. Sharff, E. Koronakis, B. Luisi, and C. Hughes, Nature (London) **405**, 914 (2000).
[2] S. K. Buchanan, Trends Biochem. Sci. **26**, 3 (2001).
[3] V. Koronakis, J. Eswaran, and C. Hughes, Annu. Rev. Biochem. **73**, 467 (2004).
[4] S. Murakami, R. Nakashima, E. Yamashita, T. Matsumoto, and A. Yamaguchi, Nature (London) **443**, 173 (2006).
[5] S. Murakami, Curr. Opin. Struct. Biol. **18**, 459 (2008).
[6] M. A. Seeger, K. Diederichs, T. Eicher, L. Brandstätter, A. Schiefner, F. Verrey, and K. M. Pos, Curr. Drug Targets **9**, 729 (2008).
[7] X.-Z. Li and H. Nikaido, Drugs **69**, 1555 (2009).
[8] K. M. Pos, Biochim. Biophys. Acta **1794**, 782 (2009).
[9] M. Kinoshita and T. Oguni, Chem. Phys. Lett. **351**, 79 (2002).
[10] M. Kinoshita, J. Chem. Phys. **116**, 3493 (2002).
[11] H. Oshima, S. Yasuda, T. Yoshidome, M. Ikeguchi, and M. Kinoshita, Phys. Chem. Chem. Phys. **13**, 16236 (2011).
[12] T. Imai, N. Miyashita, Y. Sugita, A. Kovalenko, F. Hirata, and A. Kidera, J. Phys. Chem. B **115**, 8288 (2011).
[13] R. Schulz, A. V. Vargiu, P. Ruggerone, and U. Kleinekathöfer, J. Phys. Chem. B **115**, 8278 (2011).
[14] K. Amano and M. Kinoshita, Chem. Phys. Lett. **488**, 1 (2010).
[15] K. Amano and M. Kinoshita, Chem. Phys. Lett. **504**, 221 (2011).
[16] K. Amano, H. Oshima, and M. Kinoshita, J. Chem. Phys. **135**, 185101 (2011).
[17] H. Mishima, H. Oshima, S. Yasuda, K. Amano, and M. Kinoshita, Chem. Phys. Lett. **561–562**, 159 (2013).
[18] A. L. Horwich, W. A. Fenton, E. Chapman, and G. W. Farr, Annu. Rev. Cell Dev. Biol. **23**, 115 (2007).
[19] T. K. Chaudhuri, V. K. Verma, and A. Maheshwari, Prog. Biophys. Mol. Biol. **99**, 42 (2009).
[20] S. Tanaka, Y. Kawata, G. Otting, N. E. Dixon, K. Matsuzaki, and M. Hoshino, Biochim. Biophys. Acta **1804**, 866 (2010).
[21] D. Beglov and B. Roux, J. Chem. Phys. **103**, 360 (1995).
[22] M. Ikeguchi and J. Doi, J. Chem. Phys. **103**, 5011 (1995).
[23] M. Kinoshita, Chem. Phys. Lett. **387**, 47 (2004).
[24] Y. Harano and M. Kinoshita, Biophys. J. **89**, 2701 (2005).
[25] M. Kinoshita, Chem. Eng. Sci. **61**, 2150 (2006).
[26] K. Amano, T. Yoshidome, M. Iwaki, M. Suzuki, and M. Kinoshita, J. Chem. Phys. **133**, 045103 (2010).
[27] K. Hollenstein, R. J. P. Dawson, and K. P. Locher, Curr. Opin. Struct. Biol. **17**, 412 (2007).
[28] A. Ward, C. L. Reyes, J. Yu, C. B. Roth, and G. Chang, Proc. Natl. Acad. Sci. U.S.A. **104**, 19005 (2007).
[29] M. Kinoshita, J. Chem. Phys. **128**, 024507 (2008).
[30] T. Yoshidome, M. Kinoshita, S. Hirota, N. Baden, and M. Terazima, J. Chem. Phys. **128**, 225104 (2008).
[31] M. Kinoshita, Front. Biosci. **14**, 3419 (2009).
[32] H. Oshima and M. Kinoshita, J. Chem. Phys. **138**, 245101 (2013).
[33] T. Yoshidome and M. Kinoshita, Phys. Rev. E **79**, 030905(R) (2009).
[34] H. Oshima, T. Yoshidome, K. Amano, and M. Kinoshita, J. Chem. Phys. **131**, 205102 (2009).
[35] T. Yoshidome and M. Kinoshita, Phys. Chem. Chem. Phys. **14**, 14554 (2012).
[36] J.-P. Hansen and L. R. McDonald, *Theory of Simple Liquids*, 3rd ed. (Academic, London, 2006).
[37] R. Roth, B. Götzelmann, and S. Dietrich, Phys. Rev. Lett. **83**, 448 (1999).
[38] P. Bryk, R. Roth, M. Schoen, and S. Dietrich, Europhys. Lett. **63**, 233 (2003).
[39] P.-M. König, R. Roth, and S. Dietrich, Phys. Rev. E **74**, 041404 (2006).
[40] P.-M. König, R. Roth, and S. Dietrich, Europhys. Lett. **84**, 68006 (2008).
[41] S. Asakura and F. Oosawa, J. Chem. Phys. **22**, 1255 (1954).
[42] S. Asakura and F. Oosawa, J. Polym. Sci. **33**, 183 (1958).
[43] P. Attard and G. N. Patey, J. Chem. Phys. **92**, 4970 (1990).
[44] L. Vaccaro, K. A. Scott, and M. S. P. Sansom, Biophys. J. **95**, 5681 (2008).
[45] J. C. Crocker, J. A. Matteo, A. D. Dinsmore, and A. G. Yodh, Phys. Rev. Lett. **82**, 4352 (1999).
[46] T. Yoshidome, Y. Ito, M. Ikeguchi, and M. Kinoshita, J. Am. Chem. Soc. **133**, 4030 (2011).
[47] T. Yoshidome, Y. Ito, N. Matubayasi, M. Ikeguchi, and M. Kinoshita, J. Chem. Phys. **137**, 035102 (2012).
[48] Y. Ito, T. Yoshidome, N. Matubayasi, M. Kinoshita, and M. Ikeguchi, J. Phys. Chem. B **117**, 3298 (2013).
[49] T. Uchihashi, R. Iino, T. Ando, and H. Noji, Science **333**, 755 (2011).
[50] X.-Q. Yao, H. Kenzaki, S. Murakami, and S. Takada, Nat. Commun. **1**, 117 (2010).